Proceedings of the 9th International Conference on Fluid Flow, Heat and Mass Transfer (FFHMT'22)
Niagara Falls, Canada – June 08-10, 2022
Paper No. 154
DOI: 10.11159/ffhmt22.154

Performance Analysis of an Ejector-Diffuser for Vapor Jet Refrigeration

Sankrish Jayachandran[1], T. Sundararajan[2]
[1,2]Indian Institute of Technology Madras
IIT P.O., Chennai 600036, India
sankrishj@gmail.com; tsundar@iitm.ac.in

Abstract **-** Numerical simulation of flow in an ejector-diffuser has been carried out for water-chilling application. A second throat ejector diffuser is the heart of this refrigeration system which creates a region of low (vacuum) pressure for cooling water evaporatively. To design the system and optimize its cooling performance, the effects of operating conditions and geometric parameters on vacuum suction pressure have been studied. The primary stream (air) entrains the secondary stream (water vapor) to create a low-pressure condition in the flash chamber. The primary supersonic flow needs to expand sufficiently to entrain the secondary stream and accelerate it to sonic velocity (secondary flow choking) in the throat section of the diffuser. A series of oblique shock cells will seal the low-pressure environment against ingress of atmospheric air and also help in gradual pressure recovery from the vacuum condition to the ambient. The numerically predicted results have been validated with experimental data for the optimized geometry.

Keywords: Renewable energy; supersonic flow; evaporative (vacuum) cooling; ejector-diffuser; chilled water.

1. Introduction

As per the report of IEA [1], rise in demand for cooling is already exerting enormous stress on electrical power supply in many countries, and it drives up environmental pollution as well. On an average, there are over 1.6 billion air-conditioners in use which consume more than 2000 terawatt-hours of electricity every year around the world. Heat-powered chillers are attractive alternatives. Low-grade thermal energy obtained from industrial waste heat, solar thermal, geothermal systems and power plants, can be used to power refrigeration units based on absorption or ejector principles. An ejector system is economical due to its simplicity in construction, installation and maintenance. Although ejectors were developed by the turn of the 20th century, their use for refrigeration was pioneered by Leblanc [2]. Ejector based systems are robust and have no moving parts Ejectors are employed in a wide variety of applications involving aerospace, refrigeration, power plant and desalination systems, and devices such as fuel cells, jet pumps and high-power lasers [3]–[7]

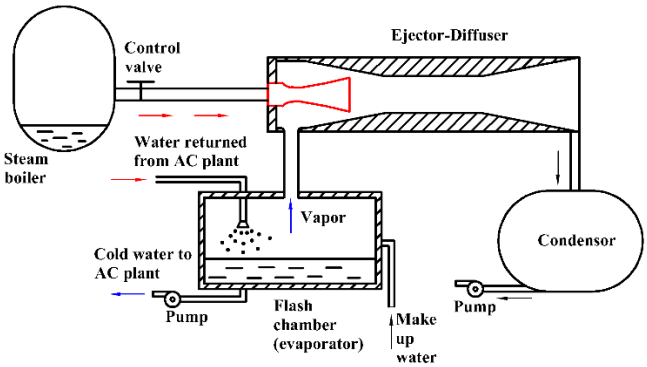

Fig. 1: Schematic of a steam jet refrigeration system. (SJRS)

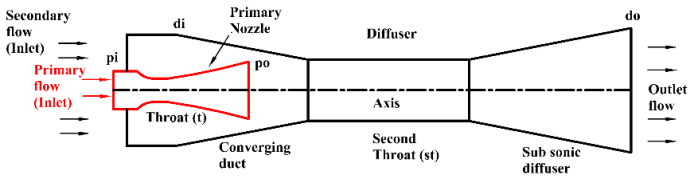

Fig. 2: Schematic of second throat ejector-diffuser (STED)

Steam jet refrigeration system (SJRS) used in water chillers is known for its environment-friendly characteristics. It works on the principle of vacuum (evaporative) cooling. Water can be made to boil below 100°C by reducing the flash

chamber pressure below atmospheric. For instance, water boils at 18 °C when the pressure on the surface of the water is at 2.06 kPa. As flash chamber pressure is reduced by ejector action, a part of the water spray vaporizes utilizing its own enthalpy for latent heat, leaving behind chilled water. For instance, if 1 kg of water evaporates out of 100 kg of water at 18°C, the remaining 99 kg will have a reduction in temperature of 5.7 °C during an adiabatic evaporation process. The major disadvantage of SJRS is that it cannot operate in sub-zero temperatures due to ice formation.

In a steam ejector, steam at high pressure and temperature from boiler expands and accelerate through a nozzle (convergent divergent primary nozzle) (Fig. 1). The high-velocity steam jet entrains the water vapour generated from the flash chamber. This creates a low-pressure vacuum in the flash chamber which helps evaporative (vacuum) cooling of water. Water is sprayed through a nozzle into the flash chamber to provide maximum surface area for cooling. The kinetic energy of the mixed stream in the diffuser is converted into static pressure and the exhaust stream is discharged to the condenser. The condensate is usually returned to the boiler. The chilled water from the flash chamber is pumped to the point of application. Essentially, the ejector acts as a thermo-vacuum compressor to draw the secondary stream and increase its pressure to that of ambient by diffuser action.

For computational simulation, the ejector-diffuser geometry is considered to have the following four parts (i) primary nozzle (ii) converging duct (iii) second throat (iv) subsonic diffuser (Fig. 2). Two types of diffuser systems are commonly employed, namely, the constant area straight ejector diffuser (SED) and the variable area second-throat ejector diffuser (STED). The STED exhibits better performance than SED as it can start performing at a lower stagnation pressure. Hence, the present ejector-diffuser geometry is based on the STED concept.

1.1. Flow and Mixing Process of Ejector.

The flow through the primary CD nozzle will be choked, if the stagnation pressure at the primary flow inlet is sufficiently high. Under certain conditions, if the back pressure at primary nozzle exit is higher than the corresponding second critical pressure, shocks will be formed in the divergent portion which give rise to subsonic flow and flow separation. The nozzle flow is said to be "unstarted" ([8], [9]) under such a condition. However, it is possible to drive the shocks out of the nozzle, either by lowering the back pressure or by increasing the stagnation pressure at nozzle inlet and the nozzle flow will be in "started" condition at this juncture. When the shock cells are driven out of the primary nozzle and they enter into the throat portion of the ejector-diffuser, another stable configuration arises. This is known as the "diffuser-started" condition. The supersonic flow (core flow) emanating from the nozzle entrains the secondary flow and creates a low-pressure region at the entrance of mixing section. The low- pressure region at nozzle exit is protected by a series of oblique shocks and expansion waves forming diamond patterns ([10]) in the diffuser duct. Since primary nozzle flow issues with high momentum, it is able to entrain the secondary vapor flow from the flash chamber and accelerate it up to choking condition ([12],[13]), within the diffuser. The mixed stream will be gradually decelerated by the oblique shock cells (followed by a weak normal shock at the end) to finally equilibrate with the ambient pressure at the exit of the diffuser.

2. Formulation And Solution Methodology

2.1. Problem Description

A laboratory scale ejector-diffuser has been designed using compressed air for primary fluid, which entrains water vapour from the flash chamber and ejects the mixed stream into atmosphere. The vacuum generated by the ejector is utilized to produce chilled water with a refrigeration capacity of 1 ton at 18°C through evaporative (vacuum) cooling. The expected vapor flow for this refrigeration capacity is 0.001458 kg/s. A scaled down model of SJRS has been fabricated and operated over a range of operating conditions, to identify its optimal performance characteristics.

2.2. Computational Methodology

The flow under consideration is axi-symmetric, compressible and turbulent in nature. The basic governing equations for the compressible flow within the ejector-diffuser are:

Continuity equation:

$$\frac{1}{r}\frac{\partial}{\partial r}(\rho r v_r) + \frac{\partial}{\partial z}(\rho v_z) = 0 \qquad (1)$$

r-Momentum equation:

$$\rho\left(v_r\frac{\partial v_r}{\partial r}+v_z\frac{\partial v_r}{\partial z}\right)=-\frac{\partial P}{\partial r}+\left(\frac{1}{r}\frac{\partial}{\partial r}(r\tau_{rr})+\frac{\partial \tau_{rz}}{\partial z}\right)+\frac{\tau_{\theta\theta}}{r} \quad (2)$$

z-Momentum equation:

$$\rho\left(v_r\frac{\partial v_z}{\partial r}+v_z\frac{\partial v_z}{\partial z}\right)=-\frac{\partial P}{\partial z}+\left(\frac{1}{r}\frac{\partial}{\partial r}(r\tau_{rz})+\frac{\partial \tau_{zz}}{\partial z}\right) \quad (3)$$

Energy balance equation:

$$\rho\left(v_r\frac{\partial}{\partial r}\left(e+\frac{P}{\rho}\right)+v_z\frac{\partial}{\partial z}\left(e+\frac{P}{\rho}\right)\right)=-\frac{1}{r}\frac{\partial}{\partial r}(rq_r)-\frac{\partial q_z}{\partial z}+\mu\phi \quad (4)$$

In the above equation,

$$\tau_{rr}=\mu\left(2\frac{\partial v_r}{\partial r}-\frac{2}{3}(\Delta\cdot v)\right) \qquad \tau_{zz}=\mu\left(2\frac{\partial v_z}{\partial z}-\frac{2}{3}(\Delta\cdot v)\right)$$

$$\tau_{\theta\theta}=\mu\left(2\frac{v_r}{r}-\frac{2}{3}(\Delta\cdot v)\right) \qquad q_r=-k\frac{\partial T}{\partial r}$$

$$q_z=-k\frac{\partial T}{\partial z} \qquad \phi=2\left(\left(\frac{\partial v_r}{\partial r}\right)^2+\left(\frac{\partial v_z}{\partial z}\right)^2\right)+\left(\frac{\partial v_r}{\partial z}+\frac{\partial v_z}{\partial r}\right)^2$$

In the above governing equations (1)-(4), μ and k denote the effective viscosity and thermal conductivity which depend on the turbulent flow field. (r,θ,z) are the spatial coordinates, v is the velocity, ρ is the density, P is the pressure, τ is the viscous stresses, q is the heat flux, ϕ is the dissipation function. The computational domain for the ejector-diffuser system (Fig. 2) was created and divided into the computational grid using ANSYS ICEM CFD 2019 R2. The governing equations were solved using ANSYS FLUENT 2019 R2, which employs finite volume method to discretize the governing equations. Density based implicit second order upwind scheme has been used to compute the flow pattern in the domain. Turbulence has been modelled using SST-k-ω model with compressibility effects included. The working fluid (air) is considered as an ideal gas.

Table 1: Parameters varied for ejector analysis.

Geometric parameters	**Value**
Ejector area ratio of A_{st}/A_t	2.25, 2.78, 4.00, 5.44, 7.11.
Distance from nozzle exit to start of second throat NXP	$0D_{po}$, $0.33D_{po}$, $0.67D_{po}$, $1.11D_{po}$, $1.67D_{po}$.
Operating condition	**Value**
Inlet pressure (kPa) P_O	200, 300, 400, 500, 600.
Secondary mass flow rate (Kg/s)	0.005277, 0.002639, 0.001319, 0.0006595, 0.000329, 0.
Exit (back) pressure (kPa)	20, 60, 100, 140, 180, 200.

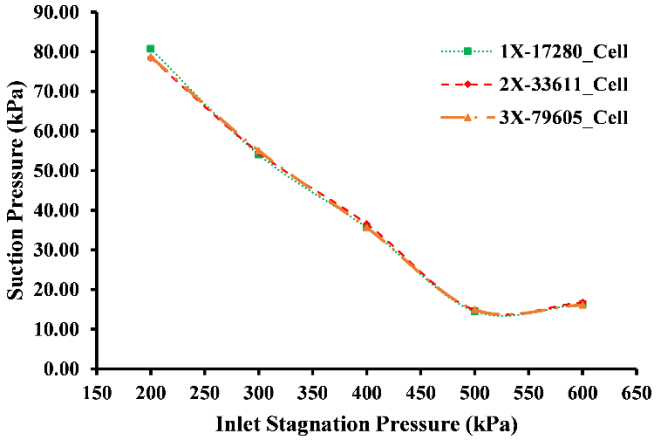

Fig. 3: Result of grid sensitivity for ejector analysis.

For upstream boundary condition of ejector, primary fluid inlet was prescribed as a pressure-inlet and the secondary flow inlet was specified as a mass flow-inlet. Pressure outlet type was applied on the downstream boundary (exit) of ejector. All walls of ejector were prescribed as adiabatic with no slip. The solution is considered converged when the difference of

mass flow rates at inlet and outlet passing through the model is less than 10^{-5} kg/s. The geometric parameters considered are: nozzle throat diameter = 6 mm, nozzle area ratio (A_{po} / A_t) = 2.25, diffuser contraction angle Θ_c = 10°, second throat length (L_{st}) = 80 mm, subsonic diffuser area ratio (A_{do} / A_{st}) = 2.25. The temperatures of both primary and secondary streams at inlet are taken as ambient (300.15 K). For the analysis, geometric parameters and operating condition are varied as listed in Table 1. To investigate the sensitivity of the grid (Fig. 3), a numerical study has been carried out for mesh sizes of 1X (17280), 2X (33611) and 3X (796605) cells. Since suction pressure was found to be insensitive to the mesh refinement beyond 2X-mesh, the 2X-mesh has been adopted for all studies. The wall y+ value in the flow field is less than 100.

3. Results and discussions

3.1. Effect of Inlet stagnation pressure

Numerical results corresponding to various inlet stagnation pressure values (200 to 600 kPa) with default value of secondary mass flow rate of 0.001319 kg/s, back pressure of 100 kPa, A_{st} /A_t of 5.44 & NXP of 0.33D_{po} are presented in Fig. 4, Fig. 5 & Fig. 6.

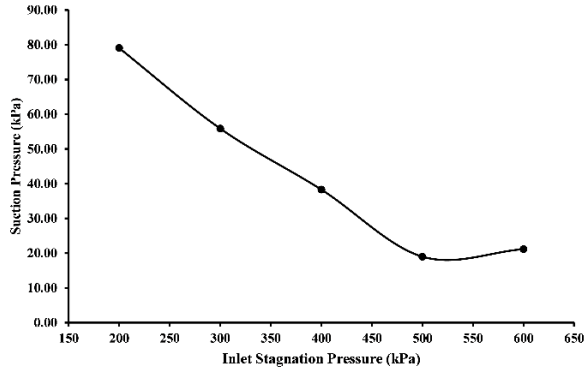

Fig. 4:Variation of vacuum level with inlet stagnation pressure

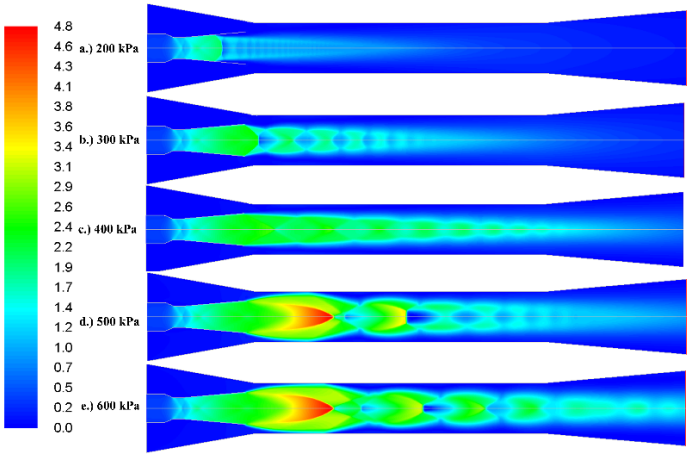

Fig. 5: Mach contour (Ma) for different inlet stagnation pressure.

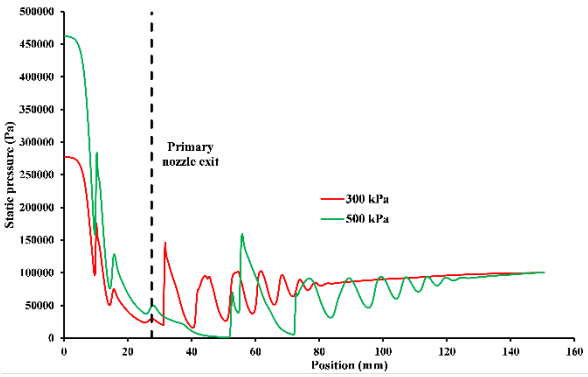

Fig. 6: Static pressure variation along axis of ejector for different inlet stagnation pressure.

From Fig. 4, it is observed that the pressure level in evaporator decreases and reaches its lowest value (~18.97 kPa) as the stagnation pressure is increased up to a critical value (~500 kPa). Beyond the critical stagnation pressure value, there is a slight increase in the vacuum pressure. The suction characteristics can be better understood using Mach number contours shown in Fig. 5. At low pressure (Fig. 5.a), the primary stream does not have adequate momentum to drive the shocks out of the nozzle. Consequently, flow separates in nozzle divergent portion. In other words, the nozzle is not “started” at low

stagnation pressure values. At critical pressure (Fig. 5.d), the primary stream expands just enough to fill the entire duct throat. The oblique shock attached to nozzle lip gives rise to a series of reflected shock cells that effectively seal the evaporator from any back flow. At the end of reflected shock cells in the diffuser duct, a weak normal shock eventually appears the near end portion of the second throat. The shock cells facilitate a gradual pressure recovery. Fig. 6 illustrates that the shock locations shift when the inlet stagnation pressure is changed

3.2. Effect of Secondary Mass Flow Rate.

For fixed primary mass flow rate of 0.0329 kg/s (inlet stagnation pressure of 500 kPa is taken as default), secondary mass flow rate is varied from 0.005277 to 0.000329 kg/s (Fig. 8.a-e) and its effect on suction pressure is studied. It is observed in that suction pressure decreases with decrease in the mass entrainment ratio (MER) from a value of 0.16 to .01.

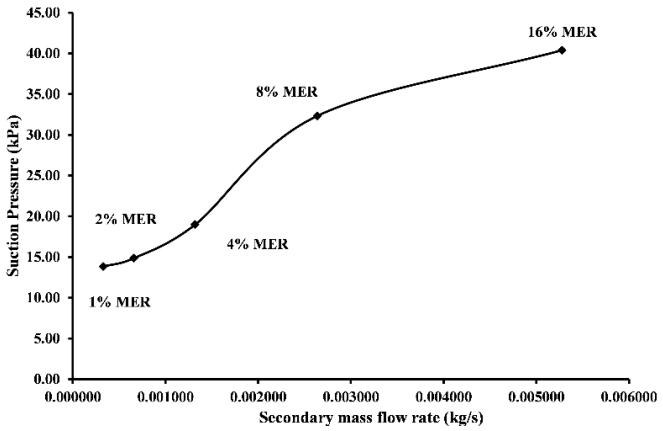

Fig. 7: Variation of suction pressure with secondary mass flow rate.

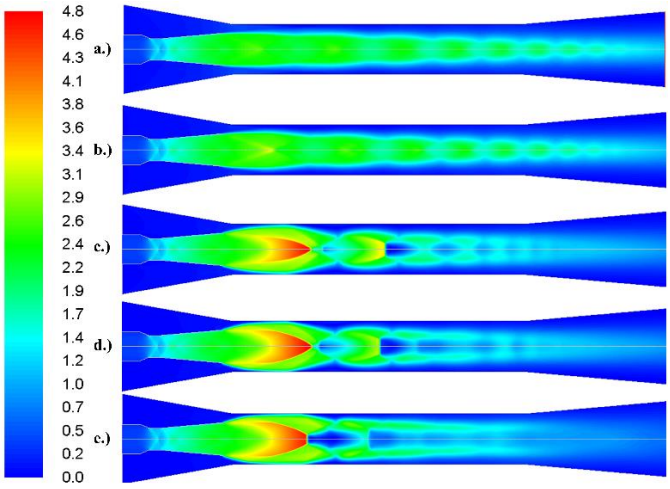

Fig. 8: Mach contour (Ma) for different secondary mass flow rate.

It can be seen from Mach number contours of Fig. 8 that the expansion angle of the under expanded flow is influenced by increasing the secondary mass flow rate. Higher secondary mass flow rate (Fig. 8.a) causes pressurisation of primary stream which lowers the expansion angle; thus, a smaller jet core and larger effective area are produced at higher MER. Lower secondary mass flow rate is indicative of high vacuum (low pressure) at evaporator. Higher secondary mass flow leads to higher total momentum of mixed stream, and shock positions move downstream.

3.3. Effect of back (exit) pressure

The results of varying the backpressure in the range 10 to 200 kPa, are shown in Fig. 9 and Fig. 10. The inlet stagnation pressure, secondary mass flow rate and geometric parameter are maintained at their default values.

It is clear from Fig. 9 that the level of vacuum remains constant at about 18.97 kPa up to a critical back pressure value of about 100 kPa; beyond the critical back pressure, the level of vacuum (low pressure at evaporator) is adversely affected and the suction pressure increases with back pressure. Considering the static pressure contours shown in Fig. 10, it is evident that the shock cells move further upstream at back pressure values above the critical value. Therefore, at higher back pressures, the evaporator performance will become poorer because of higher suction pressure.

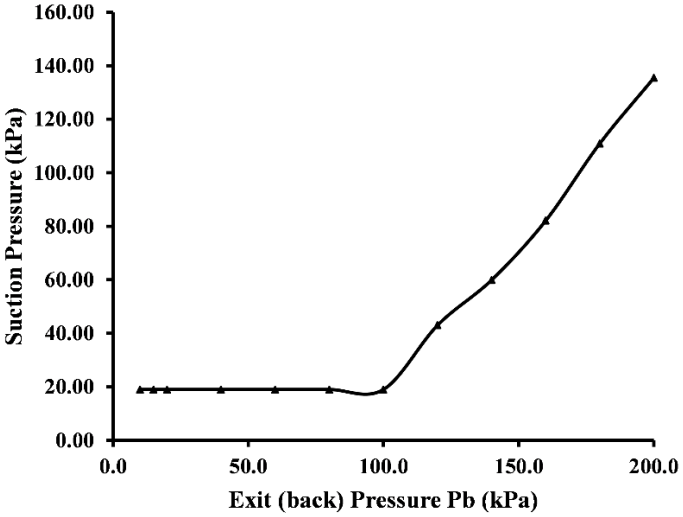

Fig. 9: Vacuum level with back pressure.

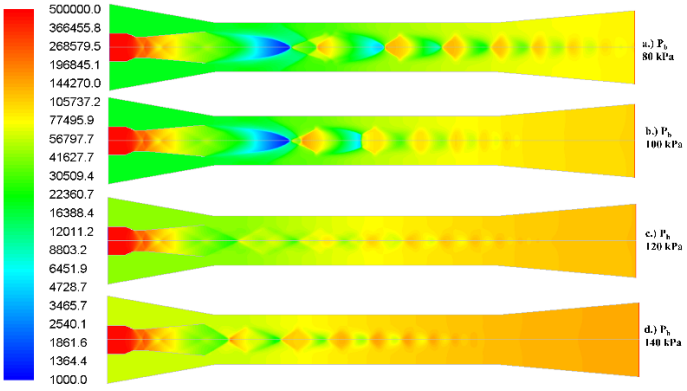

Fig. 10:Pressure contour (Pa) for different back pressures

3.4. Effect of second throat to primary nozzle throat area ratio

Suction characteristics are studied for throat area ratio A_{st}/A_t varied from 2.25 to 7.11, with other parameters held constant. The results are shown in Fig. 11 and Fig. 12.

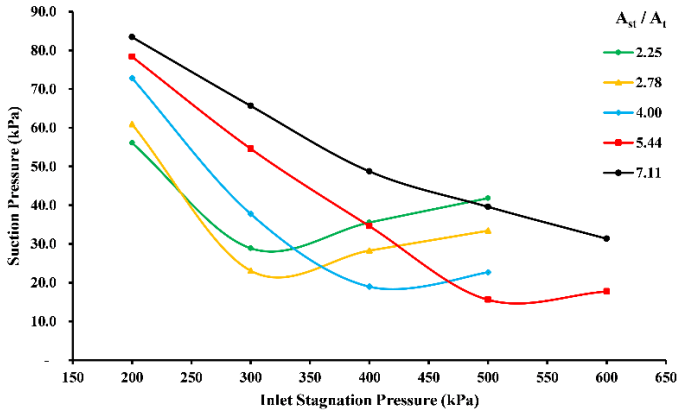

Fig. 11: Suction level with stagnation pressure for various A_{st} / A_t.

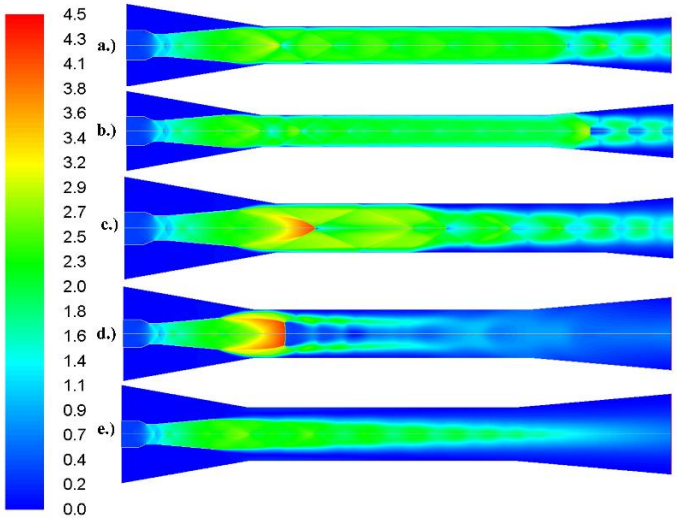

Fig. 12: Mach contour (Ma) for various A_{st} / A_t with inlet stagnation pressure of 500 kPa.

Suction pressure level decreases with increase of area ratio (of second throat to primary nozzle throat), up to a critical value and then it increases (Fig. 11), Suction pressure value of 15.6 kPa is obtained for A_{st} / A_t of 5.44. The ratio is varied by keeping the primary nozzle throat area fixed. As A_{st} / A_t is increased, it is observed that the lowest vacuum level occurs at higher inlet stagnation pressure. As ejector area ratio is increased, the gap between the primary nozzle exit and the duct increases; hence, higher momentum of primary stream is required to expand and fill the entire duct. For low value of ejector area ratio (2.25) (Fig. 12.a), suction value is high because of less annular gap. As the annular gap between primary and secondary stream is high (Fig. 12.e), the vacuum level is affected for ejector area ratio value of 7.11.

3.5. Effect of primary nozzle location

Numerical results of suction level for different primary nozzle positions are presented in Fig. 13 & Fig. 14. The location parameter L_{NXP}/D_{po} is varied from 0 to 1.67 (Fig. 14 a-e) for secondary mass flow rate of 0.0006595 kg/s and inlet stagnation pressure of 500 kPa. As the primary nozzle is moved away from the throat, suction level decreases, reaches a critical value and then increases (Fig. 13). When the primary nozzle is moved back the gap between the nozzle exit and duct wall increases. If the value of L_{NXP}/D_{po} is above 0.67 the annular gap between nozzle exit and throat of the duct increases to such an extent that the primary stream does not expand completely to seal the duct; for such a situation, the suction pressure is adversely affected. Mild variation in suction is only observed due to change in the primary nozzle position. In general, the primary nozzle should be kept close to the entrance of mixer throat for avoiding the incomplete primary jet expansion within the duct.

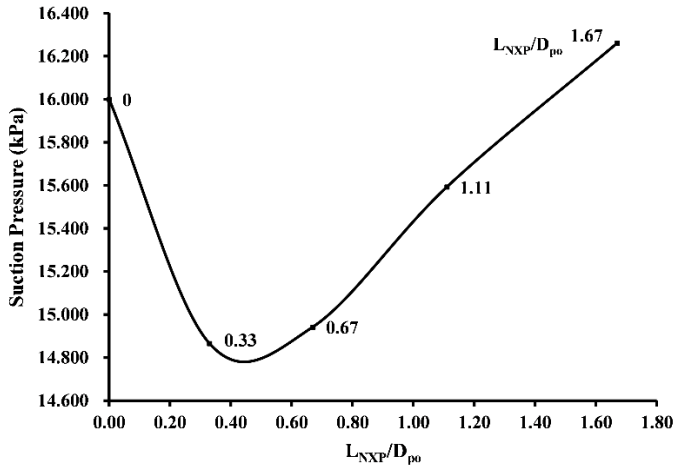

Fig. 13: Variation of suction pressure with primary nozzle location

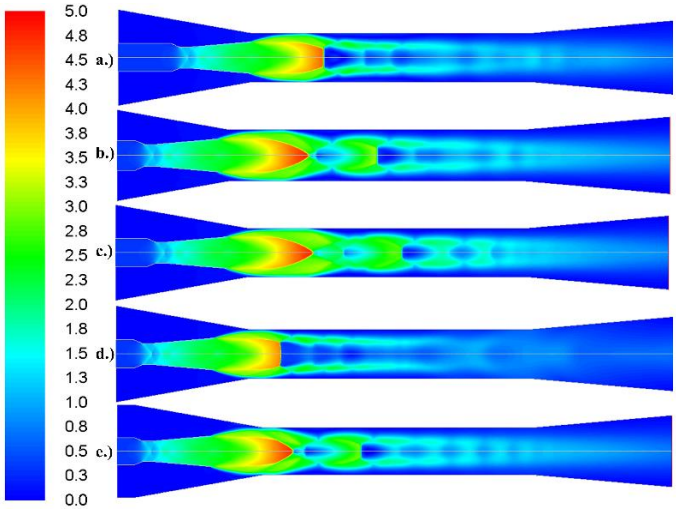

Fig. 14: Mach contour (Ma) for different primary nozzle location

3.6. Experimental results & Validation of Numerical prediction.

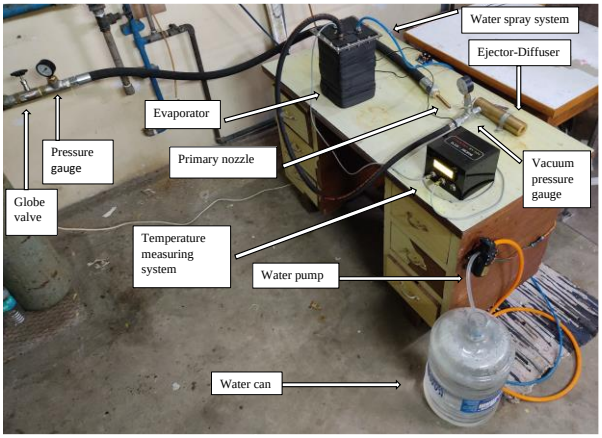

Fig. 15: Experimental setup of ejector-diffuser refrigeration system

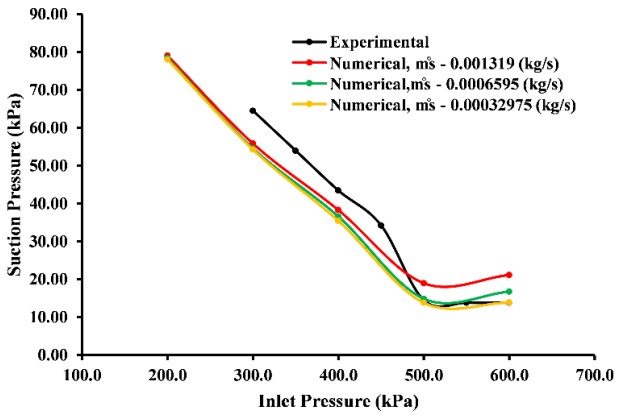

Fig. 16: Comparison of numerical and experimental results of suction pressure with stagnation pressure.

Experimental (Fig. 15) study has been carried out using the optimised ejector-diffuser dimensions and operating conditions predicted numerically. High-pressure air is supplied from a compressor line. Pressurised water is sprayed into the evaporator using an atomiser. Pressure of the inlet stream and that of entrained stream are measured. The validation of vacuum level numerically predicted for different secondary mass flow rate and that experimentally obtained are plotted in Fig. 16. Fig. 16 illustrates that fairly good agreement has been achieved for the suction pressure. For an inlet stagnation pressure of 600 kPa, suction pressure value of 14.47 kPa was achieved.

4. Conclusion

Ejector-Diffuser can be employed to create low pressure environment to enable evaporative cooling of water. Numerical prediction suggests that optimum condition is achieved when primary stream expands sufficiently to just cover the entire flow area of the diffuser duct. The train of shock cells established in the diffuser duct seal the evaporator against ingress of any backflow from atmosphere and it also helps in pressure recovery.

Acknowledgments

We thank DST, Govt of India for supporting the project on the development of Solar Cold Storage. Computational resources and the experimental facilities at TDCE lab at IIT Madras were critical supports for the project.

References

[1] "The Future of Cooling – Analysis - IEA." https://www.iea.org/reports/the-future-of-cooling (accessed Mar. 10, 2022).

[2] N. Ruangtrakoon and S. Aphornratana, "Design of steam ejector in a refrigeration application based on thermodynamic performance analysis," *Sustainable Energy Technologies and Assessments*, vol. 31, pp. 369–382, Feb. 2019.

[3] B. Peris Pérez, M. Ávila Gutiérrez, J. A. Expósito Carrillo, and J. M. Salmerón Lissén, "Performance of Solar-driven Ejector Refrigeration System (SERS) as pre-cooling system for air handling units in warm climates," *Energy*, vol. 238, p. 121647, Jan. 2022.

[4] F. Marsano, L. Magistri, and A. F. Massardo, "Ejector performance influence on a solid oxide fuel cell anodic recirculation system," *Journal of Power Sources*, vol. 129, no. 2, pp. 216–228, Apr. 2004.

[5] E. S. Ali, R. H. Mohammed, N. A. A. Qasem, S. M. Zubair, and A. Askalany, "Solar-powered ejector-based adsorption desalination system integrated with a humidification-dehumidification system," *Energy Conversion and Management*, vol. 238, p. 114113, Jun. 2021.

[6] J. Yu, H. Chen, Y. Ren, and Y. Li, "A new ejector refrigeration system with an additional jet pump," *Applied Thermal Engineering*, vol. 26, no. 2–3, pp. 312–319, Feb. 2006.

[7] G. Singhal, P.M.V. Subbarao, Mainuddin, R.K. Tyagi, A.L. Dawar, "Two-stage ejector based pressure recovery system for small scale SCOIL," *Experimental Thermal and Fluid Science*, vol. 30, no. 5, pp. 415–426, May 2006.

[8] R. M. Kumaran, P. K. Vivekanand, T. Sundararajan, K. Kumaresan, and D. R. Manohar, "Optimization of second throat ejectors for high-altitude test facility," *Journal of Propulsion and Power*, vol. 25, no. 3, pp. 697–706, 2009.

[9] R. M. Kumaran, T. Sundararajan, and D. R. Manohar, "Performance evaluation of second-throat diffuser for high-altitude-test facility," *Journal of propulsion and power*, vol. 26, no. 2, pp. 248–258, 2010.

[10] T. Sriveerakul, S. Aphornratana, and K. Chunnanond, "Performance prediction of steam ejector using computational fluid dynamics: Part 2. Flow structure of a steam ejector influenced by operating pressures and geometries," *International Journal of Thermal Sciences*, vol. 46, no. 8, pp. 823–833, Aug. 2007.

[11] A. B. LITTLE and S. GARIMELLA, "A REVIEW OF EJECTOR TECHNOLOGY FOR REFRIGERATION APPLICATIONS," *International Journal of Air-Conditioning and Refrigeration*, vol. 19, no. 01, pp. 1–15, Mar. 2011.

[12] Megalingam, A. and Babu, V ,"A numerical investigation of the compressible flow in the ejector of a vapour ejector refrigeration system," *Progress in Computational Fluid Dynamics*, Vol. 20, No. 1, pp.29–39, 2020.